Journal of Natural Disaster Science, Volume 17, *Number* 2, 1996, *pp.*99–127

LESSON FROM THE 1995 HYOGO-KEN NANBU EARTHQUAKE: WHY WERE SUCH DESTRUCTIVE MOTIONS GENERATED TO BUILDINGS?

Kojiro IRIKURA, Tomotaka IWATA, Haruko SEKIGUCHI, Arben PITARKA
Disaster Prevention Research Institute, Kyoto University Uji, Kyoto 611
and
Katsuhiro KAMAE
Research Reactor Institute, Kyoto University, Kumatori, Osaka

(Received 17 March, 1997 and revised form 30 May, 1997)

ABSTRACT

The 1995 Hyogo-ken Nanbu earthquake struck Kobe City and its surrounding, heavily populated areas, the Hanshin district, Japan, killing more than 6,400 people and destroyed more than 150,000 buildings. Surface breaks associated with the earthquake were found for about 15 km along the Nojima fault, Awaji Island; but, none were found in the Kobe area where earthquake damage was much more heavy than on Awaji. Aftershocks were distributed along already mapped active faults known as Rokko faults in the Kobe area as well as on Awaji. The most heavily damaged zones in the Kobe area did not, however, always coincide with the aftershock zones, being offset about 1 km to the south, sediment areas. Two questions had to be answered: Where are the causative faults that generated the destructive ground motions, in particular, did buried faults beneath the Kobe area rupture? In answer, the rupture process from the waveform inversion of the strong motion data shows concentrated slips in the shallower portion of the Nojima fault of Awaji Island but only in the buried portions of the Rokko faults of Kobe. The second question is why are the heavily damaged zones in Kobe not consistent with the surface fault traces associated with the buried faults. So far, earthquake damage zones are commonly believed to be directly related to causative faults, but it was not the case. We found that ground motions in the near-fault area in Kobe were characterized by two large-pulses with a duration of 1 to 2 seconds. These durations are related to the size of the asperities from the inverted slip distribution. Ground motions near the heavily damaged zones have especially distinctive pulses showing larger amplifications than those in less damaged zone as an observational fact. We consider that these large pulses may have caused the collapse of buildings and bridges in Kobe during the mainshock. We used the 3-D finite difference method to simulate near-source ground motions based on the inverted slip distributions and a 3-D velocity structure of the Kobe area. We found that impulsive ground motions of extremely large amplitudes in the period range of 1 to 2 seconds are generated and coincide with heavily damaged zones offset about 1 km from the basin edges. We concluded that these destructive motions were caused by both forward rupture directivity and basin edge effects. Special consideration of ground motions amplified by the coupling of the source and geological structure effects should be made when mapping seismic hazards in urban areas.

1. INTRODUCTION

The Hyogo-ken Nanbu earthquake of January 17, 1995, had a serious impact both in Japan and worldwide. The death toll in Kobe and adjacent cities due to the collapse of buildings and bridges, fires, and diseases induced by the earthquake has surpassed 6,400. This was the most damaging earthquake to strike Japan since the great Kanto earthquake of 1923. The fault rupture occurred in very shallow crust between the northeast part of Awaji Island and the densely populated Hanshin region. The earthquake was medium in magnitude; M_J7.2 and M_w6.9. The damage done, however, was enormous, and was unpredictable from current information available to the

KEY WORDS: the Hyogo-ken Nanbu earthquake, strong ground motion, "Damage Belt", basin edge effect, empirical Green's function.

fields of earthquake science and engineering in Japan.

The earthquake occurred on well-mapped active faults. The source region was covered by a highly-sensitive seismic network, and a continuous crustal observation station was located nearby. Nevertheless, no obvious precursory evidence appeared in the source region before the event. No practical earthquake prediction technique has yet been established, nevertheless this earthquake greatly shocked seismologists and specialists in related fields. They became aware that the present status of earthquake prediction studies had not been well publicized and that basic studies of earthquake sources and seismotectonics needed greater emphasis. But, as there poor strong motion observations existed in the source region and damaged areas, it was very difficult to determine why such severe damage occurred.

Surface breaks about 15 km long associated with the earthquake were found along the Nojima fault, Awaji Island, but not found in the Kobe area where earthquake damage was much heavier than on Awaji. Aftershocks were distributed along already mapped active faults in the Kobe area as well as on Awaji. The most heavily damaged zones, the so-called "Damage Belt", in the Kobe area, however, did not always coincide with the aftershock zones, being offset about 1 km to the south in sediment areas. This raised two questions. First, where are the causative faults that generated the destructive ground motions and did buried faults beneath the Kobe area rupture?

In the Kobe area, strong ground motions were recorded at nine stations in the near-source region. To determine the location of faulting, we investigated particle motion diagram in the near-source ground during the mainshock because particle motion should show reverse rotation on a horizontal plane on opposite sides of the fault trace. Such locations obtained from particle motion should be compared with the geodetic data in the near-source region. On the basis of the exact location of the causative faults obtained from particle motion findings, we studied the source process in which strong ground motions are generated using the waveform inversion of the strong motion data.

The second question is why are the heavily damaged zones in Kobe not consistent with the surface fault traces associated with the buried faults. It generally has been believed that damage zones are directly related to the causative faults. We realized, however, that the ground motions in the near-fault Kobe region were characterized by two large pulses with durations of 1 to 2 seconds. Ground motions near the heavily damaged zones had particularly distinctive pulses of larger amplification than those in the less damaged areas. We concluded that these large pulses may have caused the collapse of buildings and bridges in Kobe during the mainshock.

Near-source ground motions primarily are controlled by source processes such as slip distribution and rupture directivity. But, when an earthquake occurs on a basin margin fault, as in the Hyogo-ken Nanbu earthquake, basin edge effects would be very important. To examine the geological effects on ground motions near the basin's edges, we made an array observation of the aftershocks across the damage zones just after the mainshock. Reflection and refraction profiles and borehole surveys after the mainshock also have been made by various organizations to determine the detailed subsurface configurations in the Kobe area. We simulate ground motions near the basin edges from aftershocks using the 2.5-D finite difference method. We also simulated near-source ground motions from the mainshock from inverted slip distributions and a 3-D velocity structure of the Kobe area using the 3-D finite difference method.

Lastly, we estimated strong ground motions at heavily damaged sites where the mainshock was not recorded, using the aftershock records, to clarify what were the characteristics of the motions destructive to buildings and why Kobe and adjacent cities experienced such severe destruction.

2. CAUSATIVE FAULTS AND STRONG GROUND MOTIONS NEAR FAULTS.

Surface breaks of the faulting during the 1995 Hyogo-ken Nanbu earthquake extended for

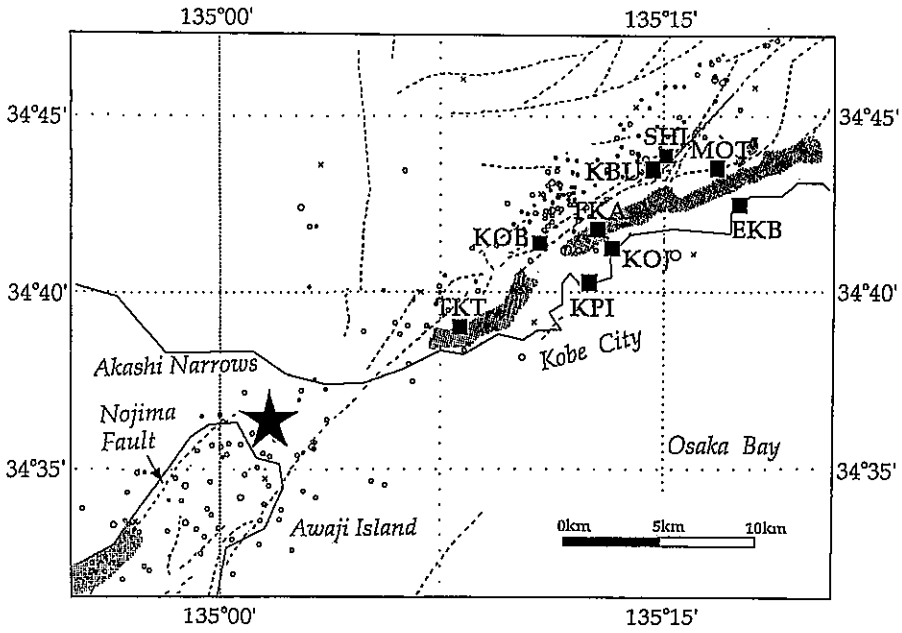

Fig. 1. Strong motion observation stations (solid squares) in proximity to the causative faults. The star and open circles indicate the respective epicenters of the mainshock and the after shocks occurring from 10.00 to 24.00 on January 17, 1995. The hatched zones show heavily damaged areas ranked as Intensity 7 (maximum intensity) by JMA (the Japan Meteorological Agency).

about 15 km along the Nojima fault, Awaji Island (Nakata and Yomogida, [1]), but no breaks were found in the Kobe area. Aftershocks were distributed along previously mapped active faults, as shown in Fig. 1. Severe damage to buildings and bridges in the Kobe area are occurred in a band along about 1 km wide running parallel to the faults but offset about 1 km to the south-east. The problem was to establish the locations of the causative faults that generated the destructive ground motions and to determine whether buried faults beneath the Kobe area ruptured.

Strong ground motion was recorded at nine stations in the near-source region in Kobe (solid squares, Fig. 1). Observed velocity and acceleration waveforms at the near-source stations are shown in Fig. 2(a) and (b), respectively. The left, middle, and right traces respectively are the horizontal component normal to the fault strike (N140°E), horizontal component parallel to it and the vertical component, taking into account the mapped active faults as the causative faults.

From the location of the mainshock hypocenter and the distribution of the aftershock, we assumed that rupture started at a depth of about 17 km under the Akashi Strait and propagated in two directions; one rupture along the Nojima Fault on the northwest shore of Awaji Island, the other along the Rokko Fault System in Kobe and adjacent cities. Preliminary analysis of the waveform inversion of the strong ground motion records showed three separate regions with relatively large moment releases; an event around the rupture starting point (hereafter, called the first subevent), a second event in a shallow part of the Nojima Fault (second subevent), and a third event deep under the city of Kobe (third subevent). Contributions from the first and third subevents are specified by horizontal solid lines over the records in Fig. 2. The contribution from the second event at stations in Kobe is very small in comparison with contributions by the other two events. Marked impulsive motions of large amplitudes are present in the fault-normal component

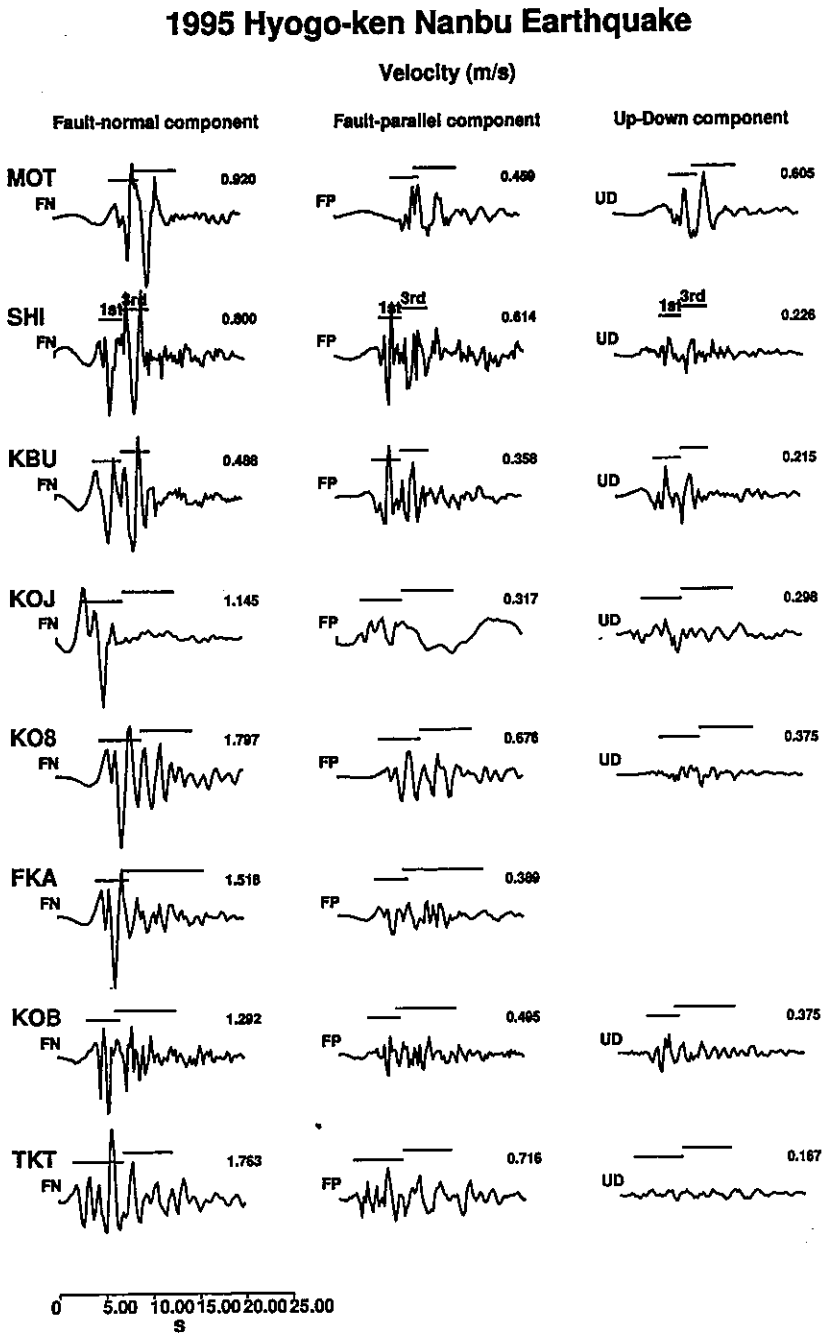

Fig. 2 (a). Observed velocity waveforms at near-source stations. Left, middle, and right: the horizontal fault-normal-component, horizontal fault-parallel-component, and vertical component. Bars, 1st and 2nd, above each waveform correspond to portions of the first and third events.

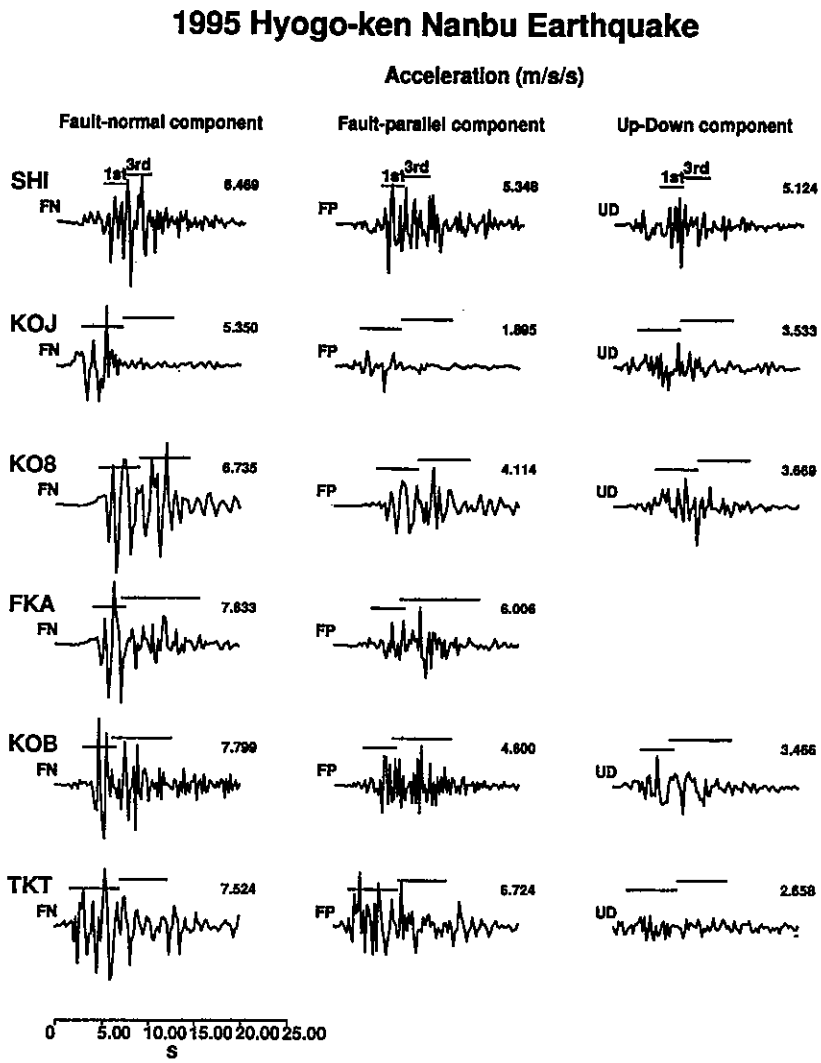

Fig. 2 (Continued.) (b). Observed acceleration waveforms at near-source stations.

at the period of about 1-2 seconds. The fault-parallel component motions are relatively small. We later show that such large pulses are generated by the forward rupture directivity as also indicated from near source recordings from several earthquakes in California (e.g. the 1966 Parkfield and the 1979 Imperial Valley earthquakes) by Heaton et al.[2] and Somerville et al.[3].

Theoretically particle motion diagrams should show reverse rotation in the horizontal plane at the two stations located on the opposite sides of the rupture area, as shown Fig. 3 (Sekiguchi et al. [4]). When the rupture causes right lateral faulting, the particle motions on one side of the rupture plane (south of the fault plane) have a counterclockwise rotation and those on the other side beyond the plane a clockwise rotation. Particle motion shows opposite rotations on the two sides, beyond and before, the tip of rupture.

Particle motion diagrams of the observed motions from the third event beneath Kobe are shown in Fig.4. At the northeastern stations of KBU, SHI, MOT, and EKB, motions from the

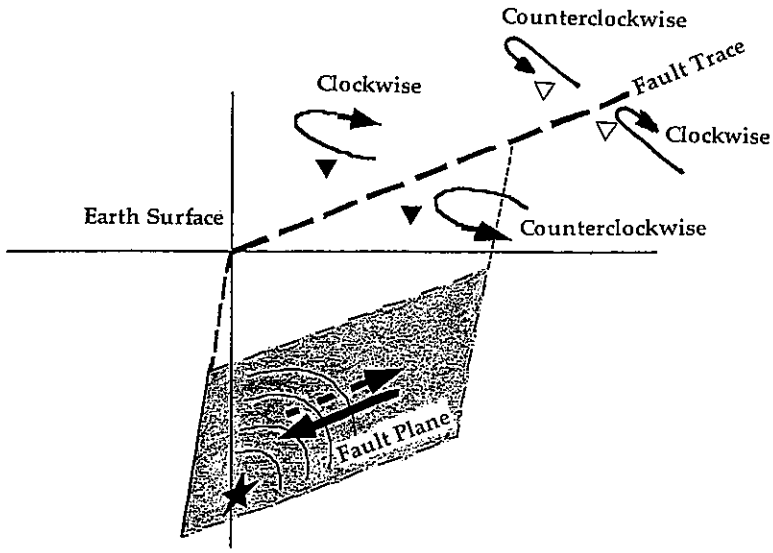

Fig. 3. Particle motion diagrams in the horizontal plane expected from finite-area faulting.

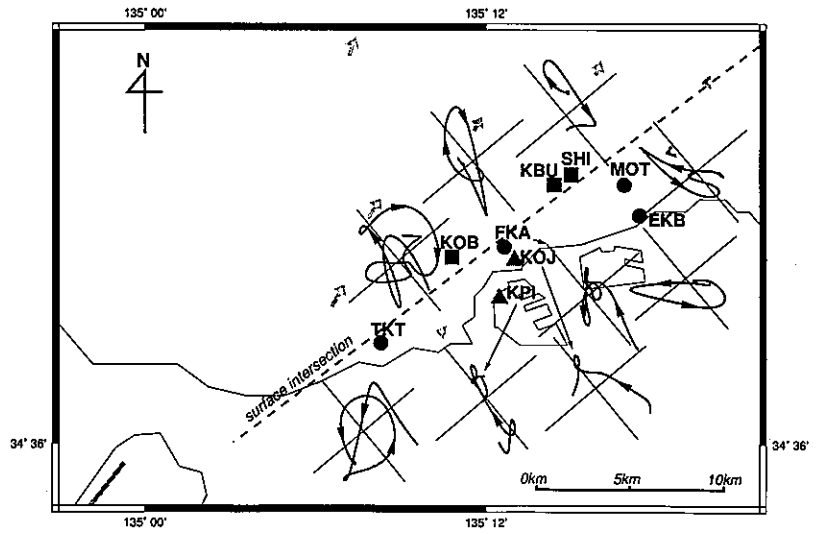

Fig. 4. Observed particle motions from the third subevent beneath Kobe. Broken line shows the intersection of the earth's surface and the extension of the fault plane. Arrows show the horizontal component of static displacements (Hashimoto et al. [6])

third event are seen as an isolated pulse (Fig.2). These four motions are classified as one of two types, the rotations at KBU and SHI being clockwise, and those at MOT and EKB counterclockwise. At the southwestern stations of TKT, KOB, KPI, KOJ, and FKA, there is no large amplitude pulse from the third event. Those stations are considered to be located behind the source area of the third event, assuming that the rupture propagated from the southwest to the northeast on the third event fault plane. In actual observation, the motions at these stations from the third

event look elongated because of backward rupture directivity. Particle motion is clockwise at KOB and counterclockwise at FKA and TKT. As a result, the surface trace of the fault plane corresponding to the third event is located to the south of KOB, KBU, and SHI, and to the north of TKT, FKA, MOT, and EKB (Fig.4). This fault trace is consistent with the known active fault lines rather than with the severely damaged zone.

Particle motions from the first event at all nine stations are clockwise, indicative that the extension of the first event fault plane is passing through the north side of the nine stations. The locations of the fault segments are delimited by the particle motion results and the geodetic data and aftershock distributions.

3. RUPTURE PROCESS FROM WAVEFORM INVERSION OF STRONG MOTION DATA

We used strong ground motion data to establish a fault plane model for the waveform inversion of the rupture process, based on the study of the rotation directions of near-source ground motions (Sekiguchi et al. [5]), as well the revised hypocenter location and aftershock distribution (Nemoto et al. submitted to J. Phys. Earth [1997]), static displacement of triangulation points (Hashimoto et al [6]), and geodetic inversion results (e.g., Ozawa et al. [7]), as shown in Fig. 5. Five segments (A, B, C, D, and E) of this fault model are constructed to correspond to active fault traces, respectively, the Nojima, Suma, Suwayama, Gosukebashi, and Ashiya faults. Segment A in Awaji is 21 km long, has a strike of 45° and dips 78° to the southeast; segment B from the hypocenter to Akashi Strait is 15 km long, has a strike of 50°, and dips 90° direction; in the Kobe area segment C is 12 km long with a strike of 233° and dips 88°; D is 12 km long, has a strike of 218.5°and dip of 88°, and E is 6 km long, has a strike of 268°, and dip of 88°, all to the northeast. All these fault planes extend from the surface to a depth of about 20 km.

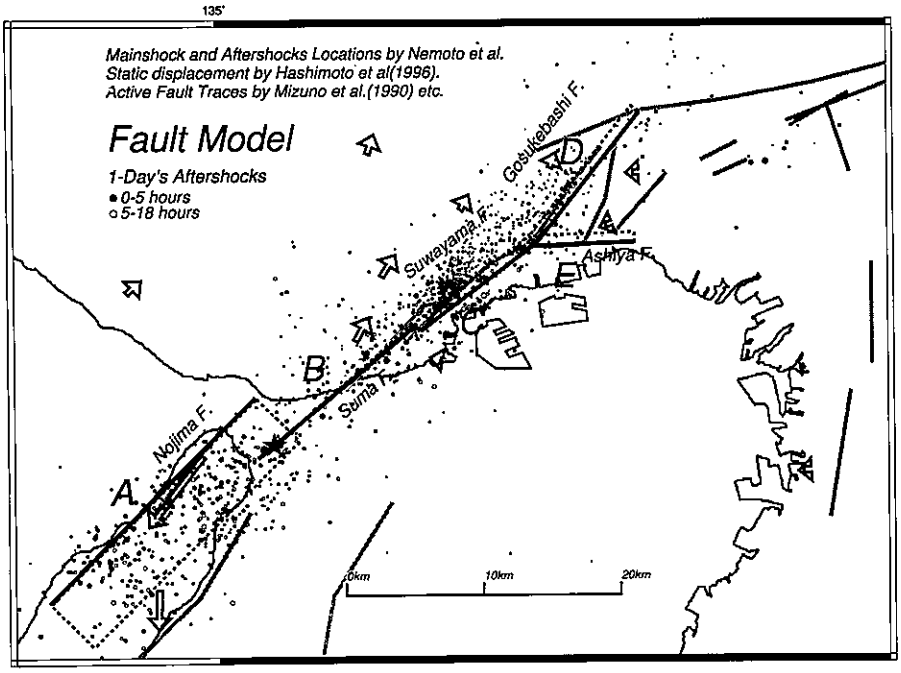

Fig. 5. Map of locations of causative fault segments. Open circles: aftershock epicenters. Arrows: static displacements by geodetic measurements.

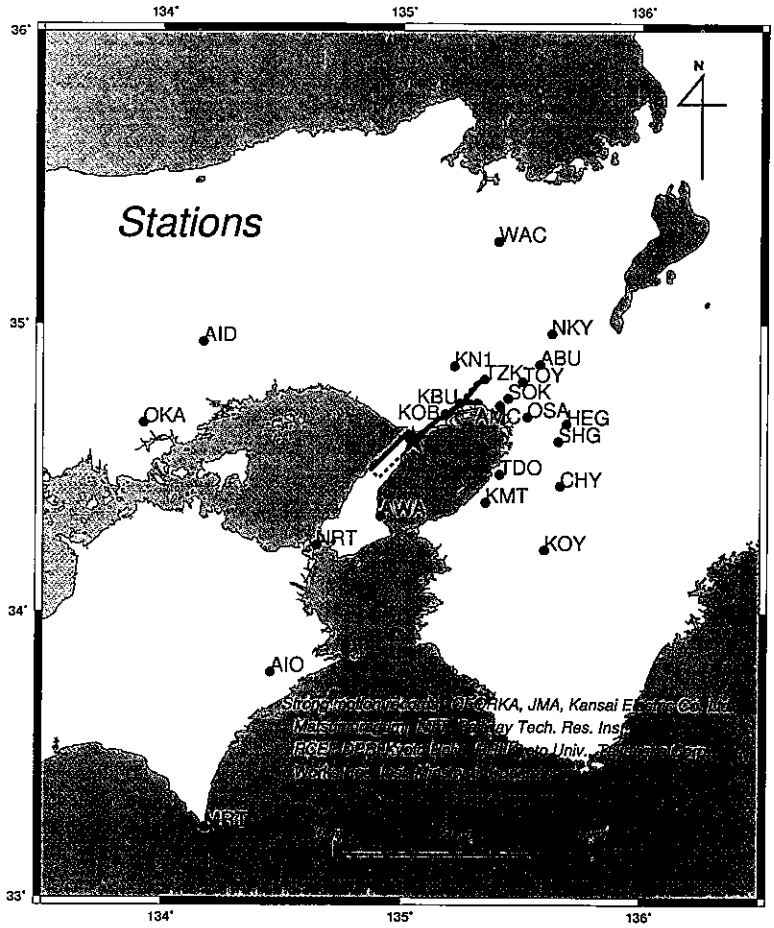

Fig. 6. Map of locations of the stations at which there were observed strong motion records used for the waveform inversion.

Sufficient evidence showing that segment E, the Ashiya fault, ruptured has not been found yet. Only a few aftershocks occurred there. Unsymmetry of static displacement vectors across the aftershock zone, however, is well explained by introducing rupture-branching to the Ashiya fault (Koketsu et al. [8]). The near-source ground motion simulation based on the source process without the Ashiya fault branching does not well explain the "Damage Belt" that extends to Ashiya and Nishinomiya (Pitarka et al. submitted to Bull. Seis. Soc. Am, 1997). These observations suggest there may have been dislocation on the Ashiya fault.

We performed waveform inversion of the strong ground motion seismograms obtained at 23 stations ranging from almost 0 to about 150 km from the earthquake source (Fig.6). Azimuthal coverage is fairly good for an epicentral distance of more than 40 km. Displacement waveform data bandpass-filtered between 0.1 and 1.0 Hz, obtained from the strong motion records, were used. The multi-time window linear waveform inversion by Hartzell and Heaton [9] was applied.

The rupture is considered in the inversion to start at the hypocenter (depth: 16.37 km), indicated by the star in Fig. 5, located at a bend of the known active faults under the Akashi Strait and to propagate bilaterally to the southwest on segment A and to the northeast on segments B, C, D, and E. We obtained the distributions of the total slip vector in Fig. 7. A right-lateral strike slip was dominant over the fault. The time progression of rupture in terms of moment release

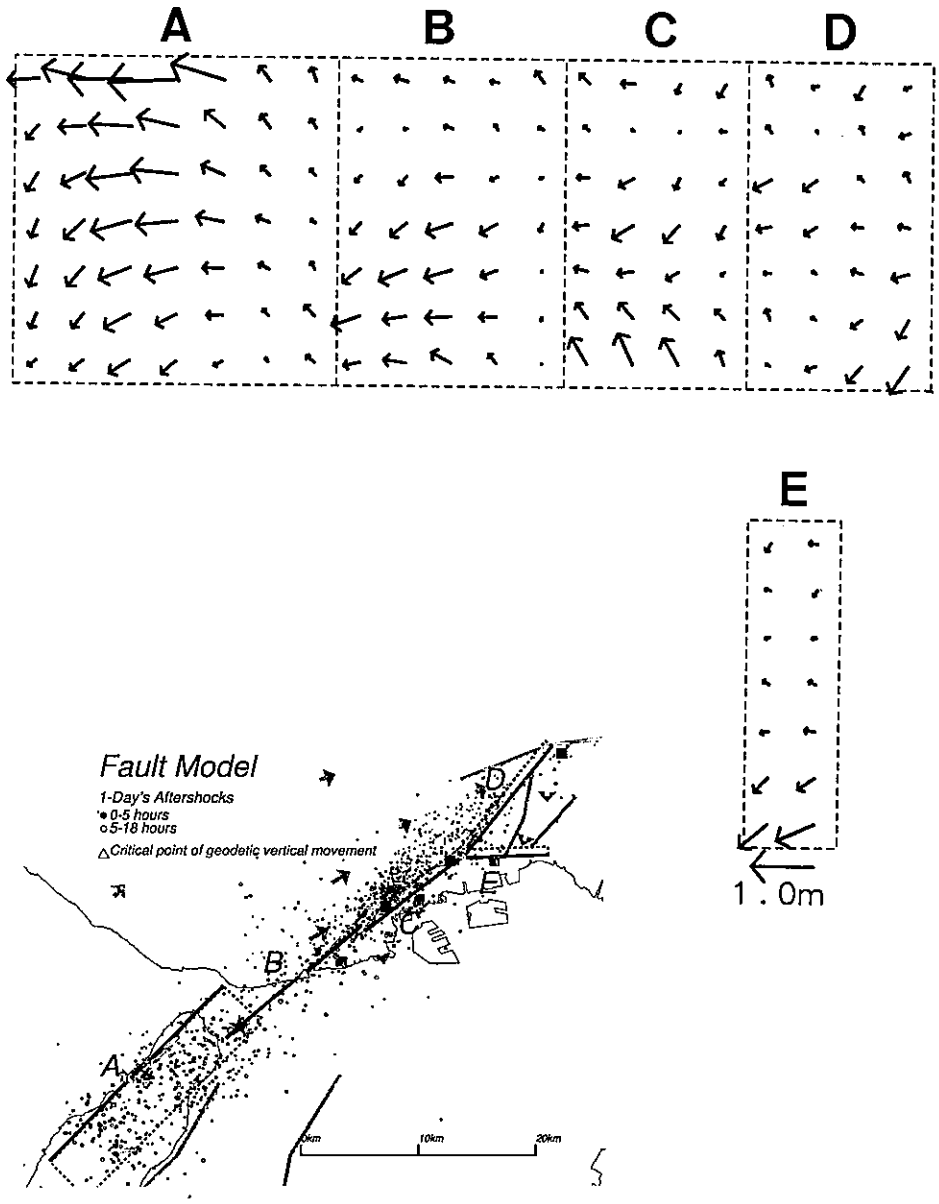

Fig. 7. Distribution of the total slip vector (upper) obtained from waveform inversion using strong ground motion records.

is shown in Fig. 8. The synthetic waveforms for the inverted model agree well with the observed ones, as shown in Fig. 9.

The results of the slip distributions shows three large asperities; beneath the Akashi Strait, along the Nojima fault, and beneath Kobe, which already have been reported by Sekiguchi et al. [5] and by several other inversion studies made of this earthquakes (Ide et al. [10]; Yoshida et al. [11]; Wald [12]). In this study, we obtained two other possible asperities; in the deep parts of the Ashiya and Gosukebashi faults. In particular, the moment release density on the Ashiya segment is high.

We made several tests to examine the validity of the Ashiya fault slip. We first did waveform

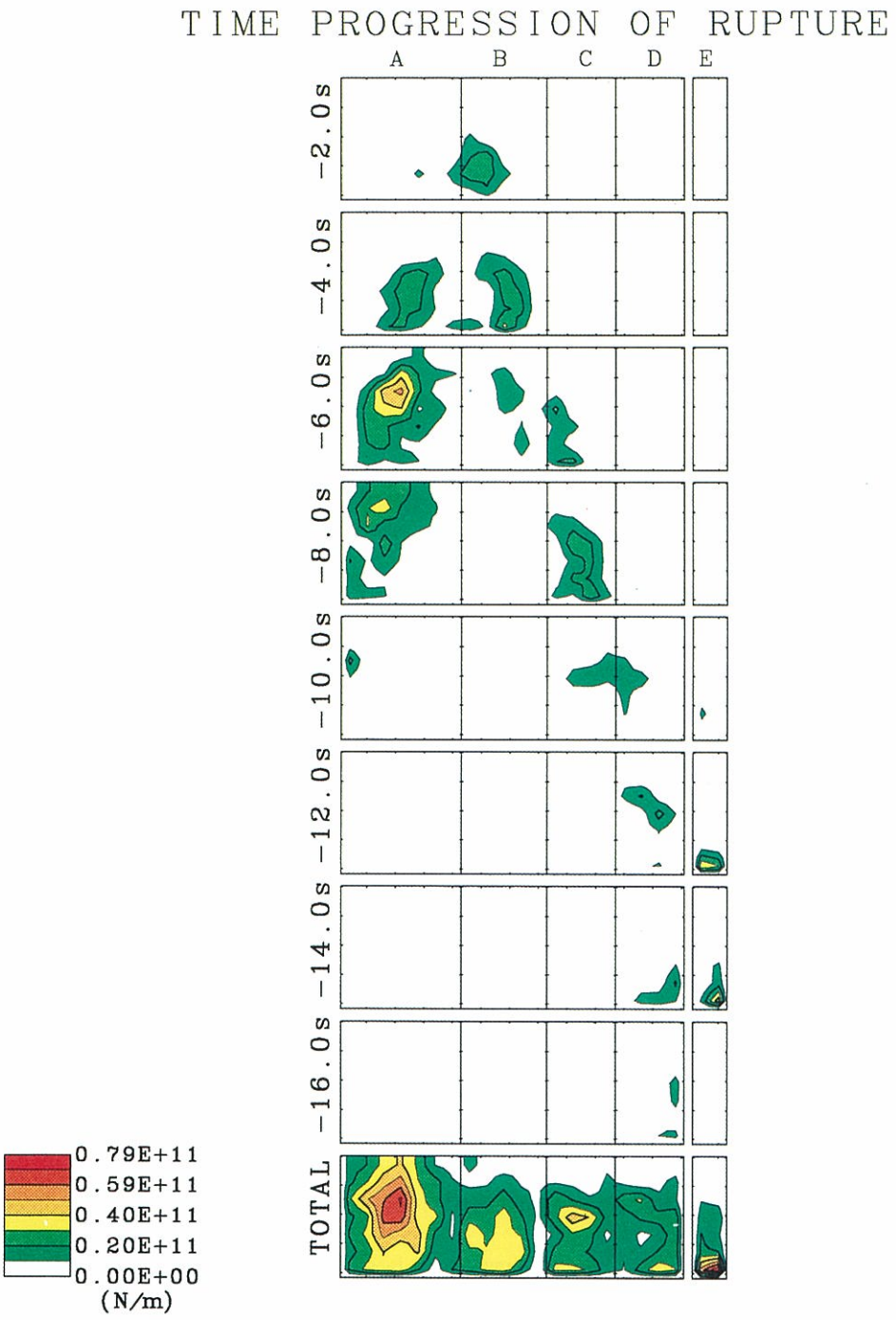

Fig. 8. Time progression of rupture (moment release) and the distribution of total moment release. Each time window is 1.5 seconds.

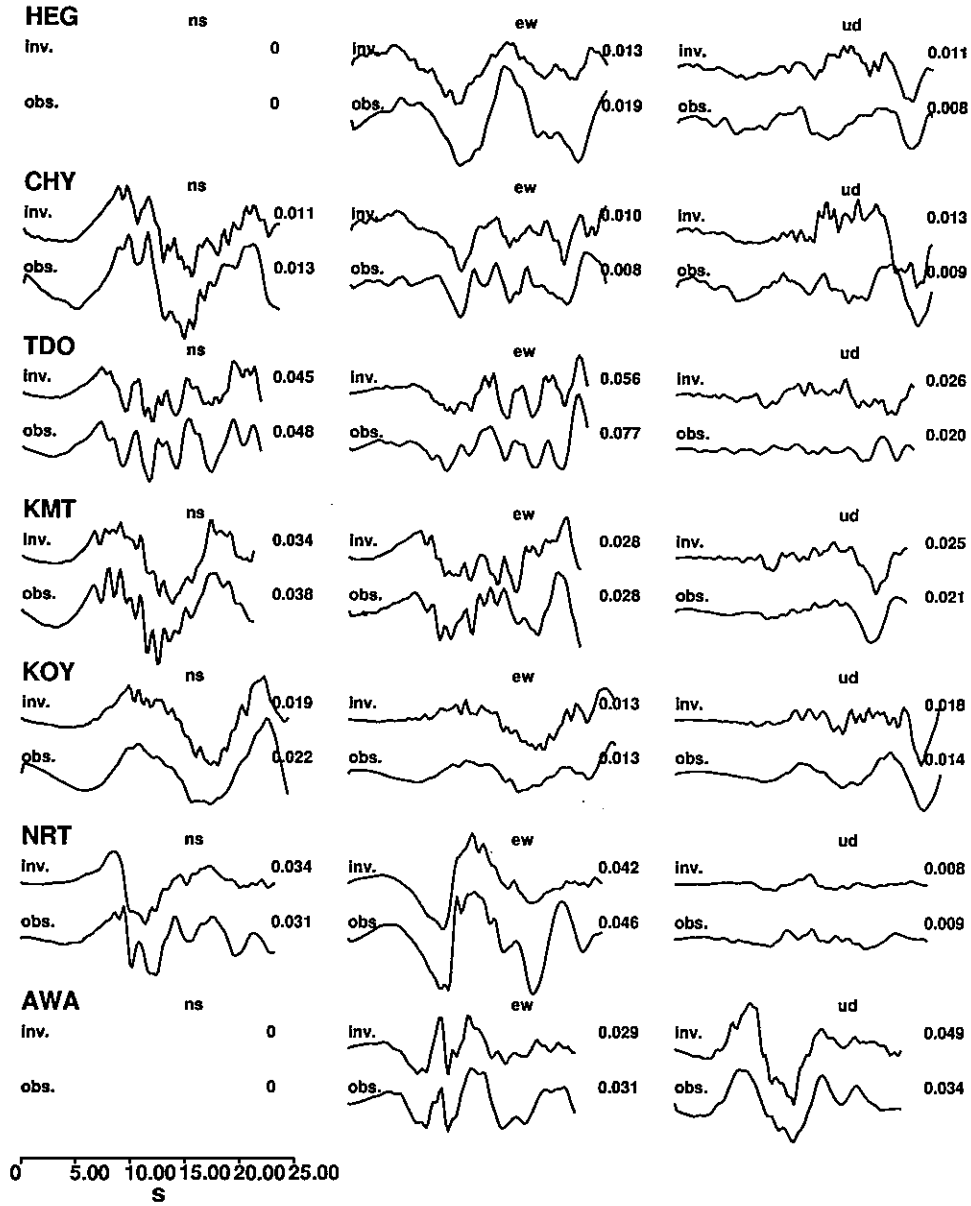

Fig. 9. Comparison of synthetic (upper) and observed (lower) displacement waveforms.

inversion using synthetic data from the three asperities on segments A, B, and C with noises (5 to 20 %) as data. Results showed that data with even 20% noise scarcely made such a strong ghost asperities on the deep part of the Ashiya segment, although small ghost slips appeared on the segment. We then examined the affects of misestimation of the shallow layer characteristics at the stations in the Osaka basin. Results inverted based on misestimation of Green's function did not show strong ghost asperities.

The two remarkable pulses seen in the fault-normal component of the observed velocity seismograms (Fig. 2) were from the first and third subevents, not from the second. These pulses clearly were generated from the forward rupture directivity effects as indicated by Heaton et al.

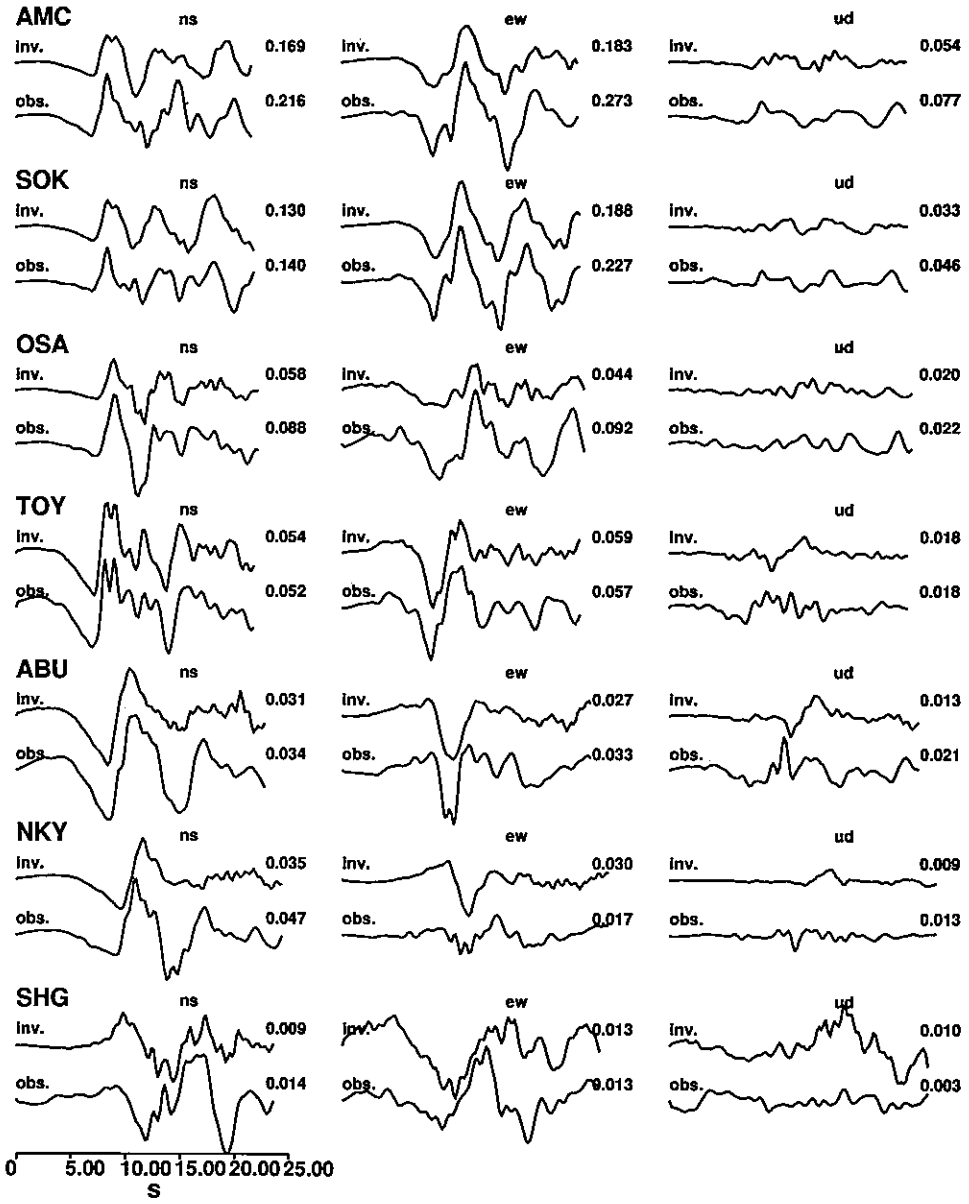

Fig. 9. (Continued.)

[2]. The pulse width is related to the size of the subevents; i.e., asperity size. Contribution to the seismograms from the asperity on the Ashiya segment would not be marked, even if such an asperity exists.

4. ARRAY OBSERVATION OF GROUND MOTIONS FROM AFTERSHOCKS ACROSS THE DAMAGE BELT

To study the characteristics of the strong ground motions related to damage distribution during

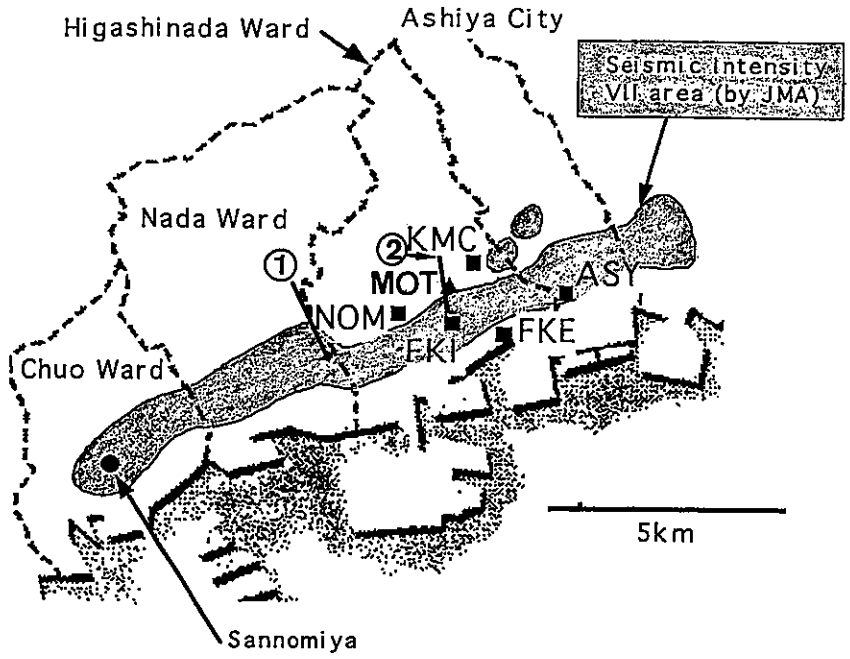

Fig. 10. Map of severely damaged zones (shaded), permanent (triangle) and temporary (squares) observation stations in Higashinada Ward, Kobe City. The temporary stations were deployed for aftershock observations. Thick solid lines: the locations for seismic profiling, 1: Ishiyagawa line and 2: Okamoto line.

earthquake, we made an array observation of ground motions just after the mainshock (Iwata et al. [13]). Strong motion seismometers were deployed in an array from the fault zone on a hill to the seaside (Fig. 10) in Higashinada ward, across the heavily damaged zone (the "Damage Belt"). KMC is located on rock, close to the northern edge of the Osaka basin, whereas MOT, NOM, FKI, and ASY are on alluvium, and FKE is on reclaimed land. Seismic reflection profiles near the Higashinada array were made in two lines indicated by the thick, solid lines in Fig. 10. The cross sections are shown in Fig. 11. The basin edge has a step-like geometry. The bedrock consists mainly of granitic rocks with an S wave velocity of about 3.2 km/s (Kagawa [14]).

Observed acceleration records from an aftershock with magnitude 3.2 are shown in Fig. 12. The sediment site records show considerably larger amplitudes in both the NS and EW components, except for those at MOT located very close to the basin's edge.

Ground motion amplification is largest at FKI in the central part of the damaged zone and decays at sites outside of the heavily damaged zone. There appears to be a good correlation between the large ground motion area and the heavily damaged zone.

We modeled the 2-D velocity structure in this area for simulation. The topographical shape of the bedrock was constructed from based on the seismic reflection profiles. Three layers, with S wave velocities of 300, 500, and 1,000 m/s in the sediment area were given from the Osaka basin structure model by Kagawa et al. [14]. The uppermost layers, at a depth of a few meters, have S wave velocities from 125 to 250 m/s based on the P-S wave velocity logging and shallow S-wave reflection survey. Because of computational limitations, we assume that the shallowest sedimentary layer has a shear wave velocity of 300 m/s and neglect shallower soft layers with lower velocities.

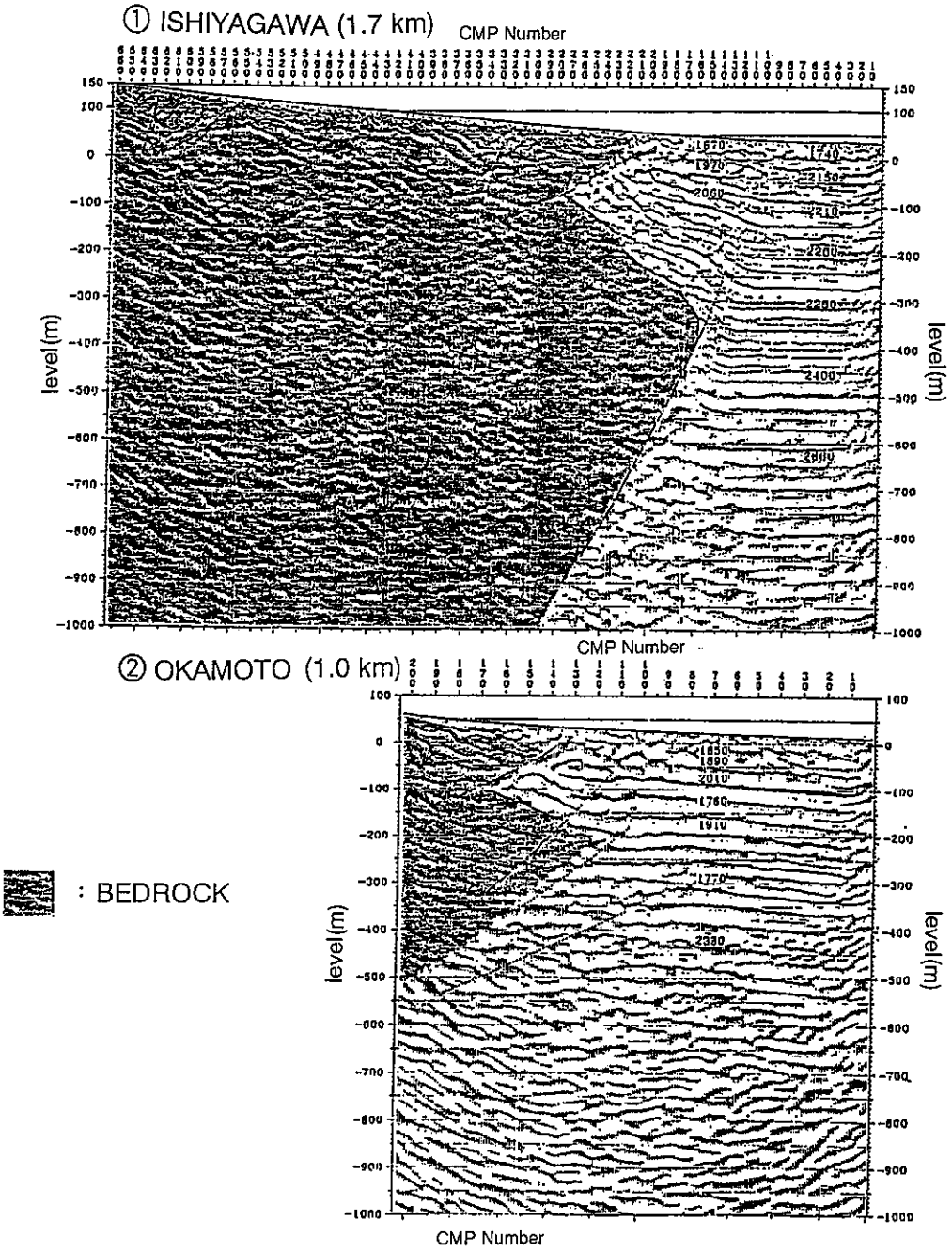

Fig. 11. Seismic profiles at the Ishiyagawa and Okamoto lines. The dark color indicate rock. Numbers in the profiles are estimated P wave's velocities.

We used the so-called 2.5D finite difference (FD) schemes (Pitarka and Irikura [15]) to simulate propagation of the seismic waves in the heterogeneous structure beneath the Higashinada array (Pitarka et al. [16]). The synthetic and recorded velocity seismograms, bandpass-filtered at

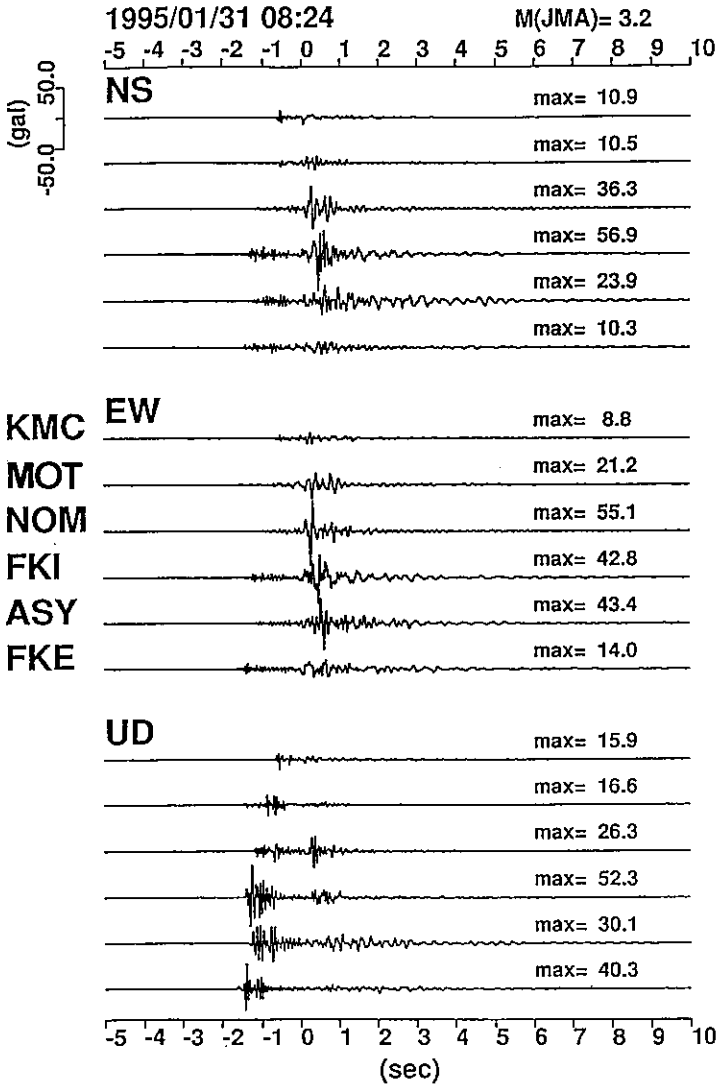

Fig. 12. Observed ground accelerations at the stations shown in Fig. 8 from the M 3.2 aftershock (Jan. 31, 1995) with a hypocenter located about 0.7 km north of KMC and about 3.8 km deep.

0.1–2 Hz were compared (Fig. 13). There is good agreement between the simulated and recorded waveforms at all the sites. Spatial amplitude variation is reproduced fairly well; but, the modeling underestimated the S wave amplitudes at FKI and FKE by about 50 %. This suggests that the shallower layers with lower S wave velocities, not included in the model, may amplify ground motions more at these sites. Their effect must be accounted for when making a more realistic model of ground motions in this area.

To gain insight into how the basin edge affects ground motions, we show snapshots of the simulated wavefield in Fig. 14. They represent the SH wave components generated by a point source with a strike-slip mechanism corresponding to the aftershock. The snapshot at 1.2 sec shows the wavefront of the direct SH wave that has just entered the basin while propagating to

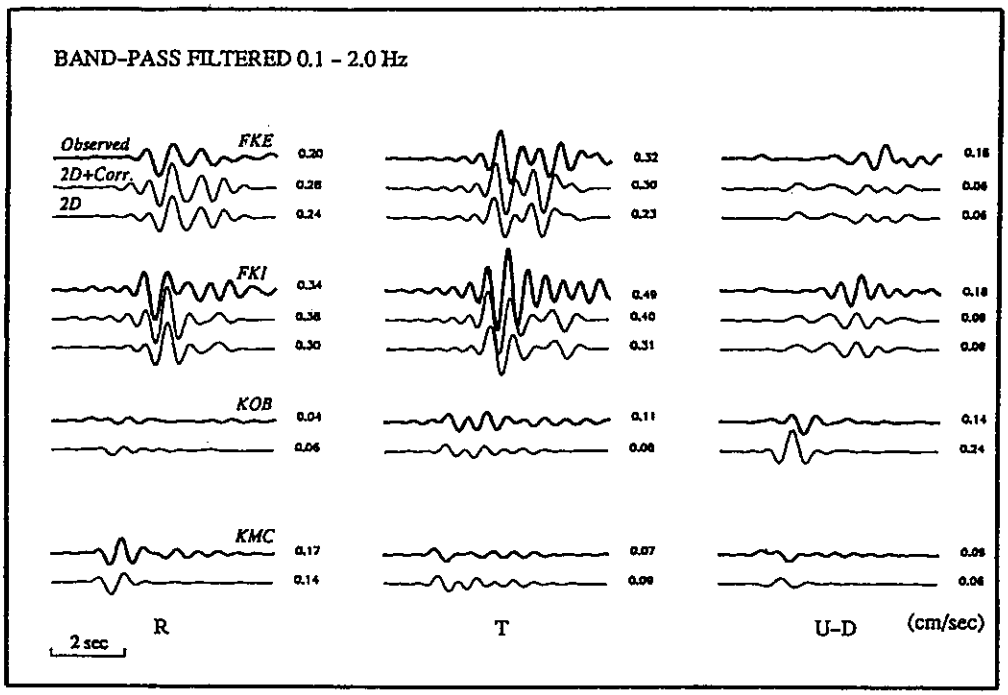

Fig. 13. Comparison between the synthetic velocity seismograms and the observed seismogram from the M 3.2 event. 2D: synthetic for the 2D structure model and 2D'Corr: synthetic for the 2D model corrected by the 1D soft surface layer model. R: horizontal radial, T: horizontal transverse, and U-D: vertical components. The seismograms are band-pass-filtered between 0.1 and 2.0 Hz.

the surface. Two distinct waves are present at 2.0 and 2.2 sec. The former, a diffracted wave originating from the wave moving upward through the bedrock, propagates horizontally in sediments with low phase velocities close to the S wave velocities of the sediments. The latter wave is the direct wave that propagates almost vertically upward through sediments at the S wave velocity of the sediments. These two waves are superposed at about 2.8 sec at a distance about 0.7 km from the basin edge that corresponds to the northwest edge of the "Damage Belt". Their constructive interference, which causes the amplification of ground motion, is effective within a zone of about 1.4 km, offset from the basin edge by about 0.7 km. After 3.2 sec the latter waves are reflected downward at the surface of the sediments and begin to separate from the former waves propagating horizontally.

From this analysis we concluded that the constructive interference of the direct S waves (propagating almost vertically upward) with the diffracted S waves (generated at the basin's edge and propagating horizontally along the surface), causes the amplification of ground motions in a narrow zone about 1.4 km wide.

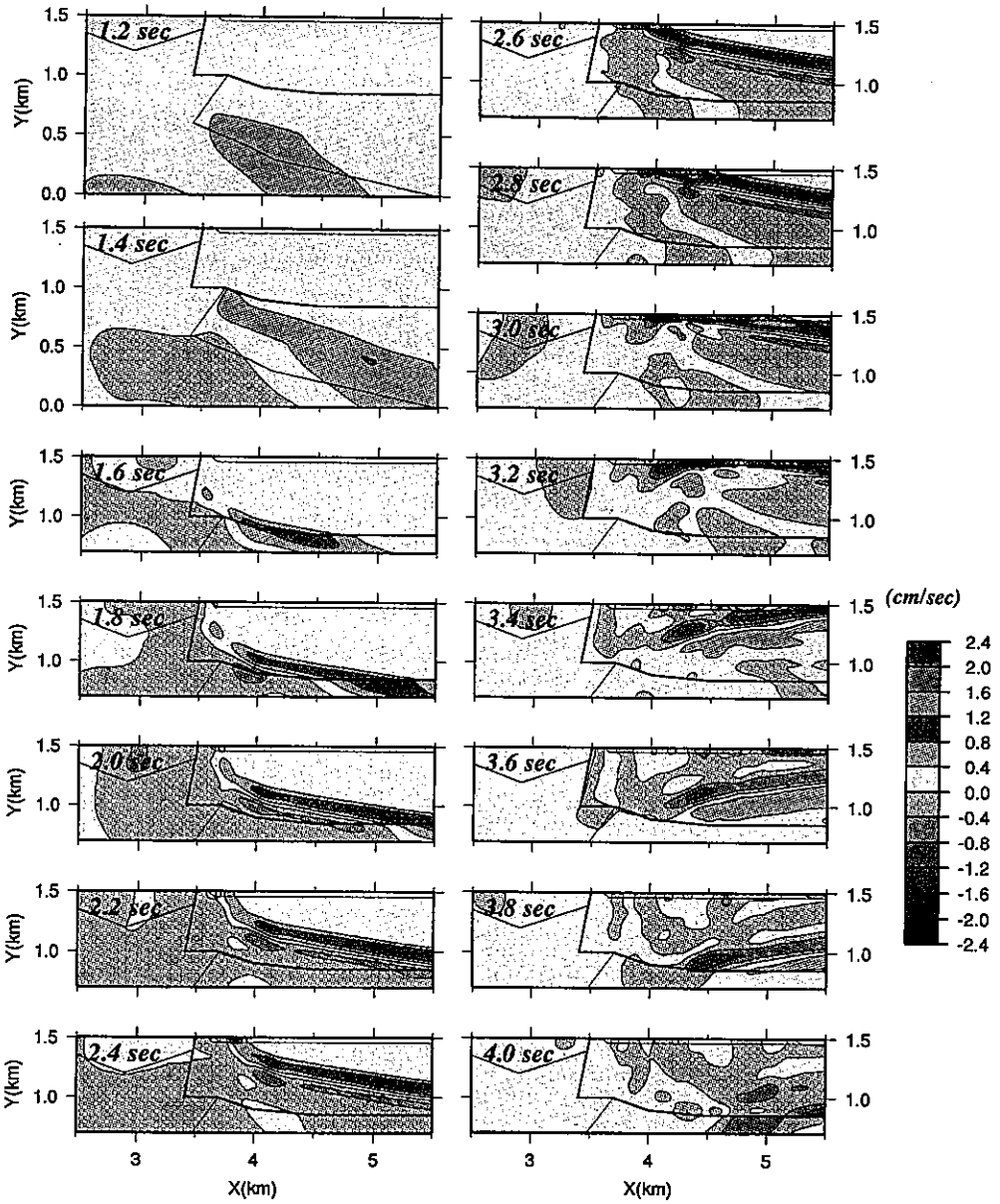

Fig. 14. Snapshots of synthetic velocity motions from the M 3.2 aftershock (Jan. 31, 1995) using the 2.5 Finite Difference Method. The lapse time, T, for each snapshot is given at upper left, from 1.2 to 4.0 sec. The amplitude levels are plotted in the right columns.

5. WHY WAS THE DAMAGE BELT PRODUCED?

The most dramatic feature of this earthquake was the "Damage Belt" that was offset by about 1 km and nearly paralleled the fault zone. Some geologists thought that the heaviest damage in Kobe was directly related to movement of buried faults just beneath the sediments. This

idea, however, has several drawbacks: there were few aftershocks beneath the damaged zone, it is not consistent with geodetic data, and there is no matching of near-source particle motions. The causative faults we obtained well match the known active fault zone. We need, therefore, to discuss why the damage belt was produced.

Three Dimensional Structure in the Kobe Area

The Kobe area is characterized by a complex geology, being in proximity to numerous active faults. After the earthquake, the subsurface geological structures in this region have been made clear by several organizations on the basis of refraction and refraction profiles and bore-hole information (CEORKA, 1995; The Committee for Active Fault Surveys in Hanshin Area, 1996; Geological Survey of Japan [17]; Iwata et al. [18]) and Bouger anomaly analysis (Kobayashi et al., [19]). We constructed the subtopography of the bedrock beneath the Kobe area as shown in Fig. 15, from this information. The bedrock consists mainly of granitic rocks and partially of volcanic and sedimentary rocks. These rocks are widely exposed in the surrounding mountainous regions. The S wave velocity of the bedrock is about 3.2 km/s (Kagawa et al. [14]). Sediments overlying the bedrock in the basin area consist of the Osaka Group, upper Pleistocene and Holocene alluvial deposits (Nakagawa, et al. [20]), that rapidly become deep with reverse faults. In the Kobe area they are represented by three distinctive layers that dip slightly to the south. The maximum thickness of the sediments in the area of interest is about 2.1 km. The Osaka Group and the upper Pleistocene layers have respective average S wave velocities of 0.55 and 1.0 km/s (Kagawa et al.,1993). A large part of the basin is partially covered by very soft soils with a high water content and an S wave velocity of 0.1 to 0.25 km/s in the upper few meters. The soils along the coast are mainly those of reclaimed land that is susceptible to nonlinear behavior or liquefaction due to strong ground shaking (e.g. Aguirre and Irikura [21]).

The 3-D Simulation of Near Source Ground Motion

We simulated the strong ground motions in the Kobe area from a kinematic model of the fault rupture using the 3-D finite-difference method (Pitarka and Irikura [22]). Our purpose is to show the interaction between the source effects, in particular rupture directivity effects, and geological effects such as the basin-edge and surface geology in the observed near-source ground motions.

A rough, three dimensional velocity model with a spatial resolution that satisfies the band limited frequency content (0.2–1.0 Hz) was constructed for our finite-difference simulation. The model has a single sedimentary layer with an S wave velocity (Vs) of 0.8 km/s, a P wave velocity (Vp) of 1.6 km/s, a density (ρ) of 2.1 (10^3kg/m^3), and quality factor (Q) of 80. The adopted S wave velocity is estimated by averaging the velocities of the three sedimentary layers in the Osaka basin. The velocity structure of the bedrock is modeled by the three horizontal layers with the layer parameters [Vs(km/s), Vp(km/s), ρ(10^3kg/m^3), Q, and thicknesses(km)] of (3.2, 5.5, 2.6, 300, 4), (3.5, 6.0, 2.7, 400, 17.8), and (3.9, 6.7, 2.8, 500, infinite).

We simulated near-source ground motions with the 3-D FDM taking into account the three-dimensional structure described above and the source process obtained in this study. The distributions of the vectors of the horizontal peak ground velocities are shown in Fig. 16. The fault-normal components are markedly larger than the fault-parallel and vertical ones. The peak amplitude distributions of the ground velocities are shown in Fig. 17. The concentrations of the horizontal peak velocities larger than 40 cm/s are elongated in a narrow zone offset from the fault traces by about 1 km, similar to setting of the "Damage Belt". The absolute amplitude levels of the peak velocities might be somewhat smaller than actual ones because the synthetics are

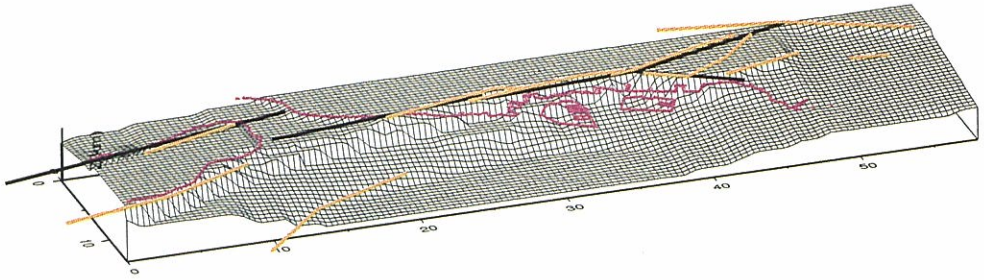

Fig. 15. The bedrock topography in the Kobe area used in the 3-D modeling.

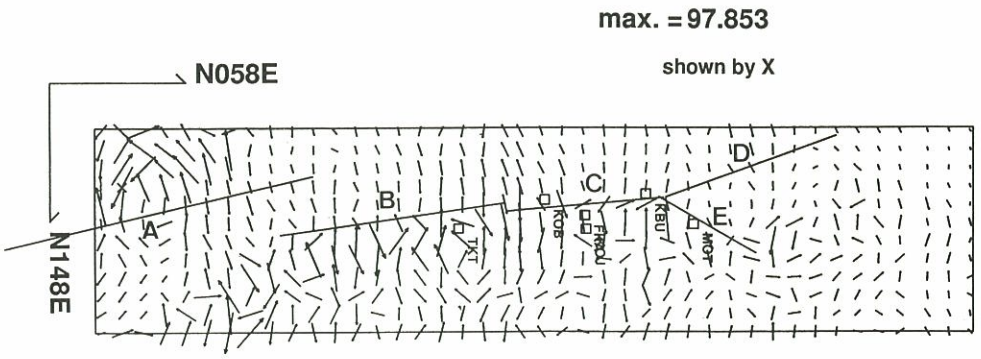

Fig. 16. Distribution of vectors (peak velocity) of simulated ground motions on the surface in the basin structure model (Fig. 15) taking into account the rupture process (Fig. 7).

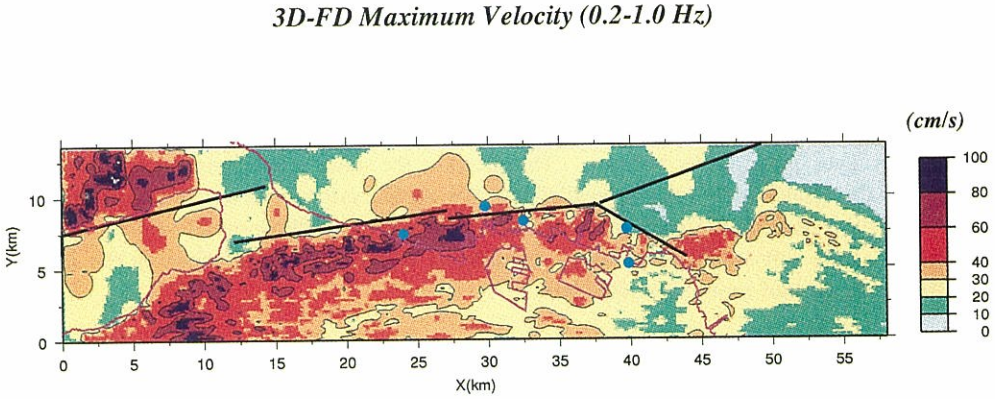

Fig. 17. Simulated peak velocity distribution on the surface.

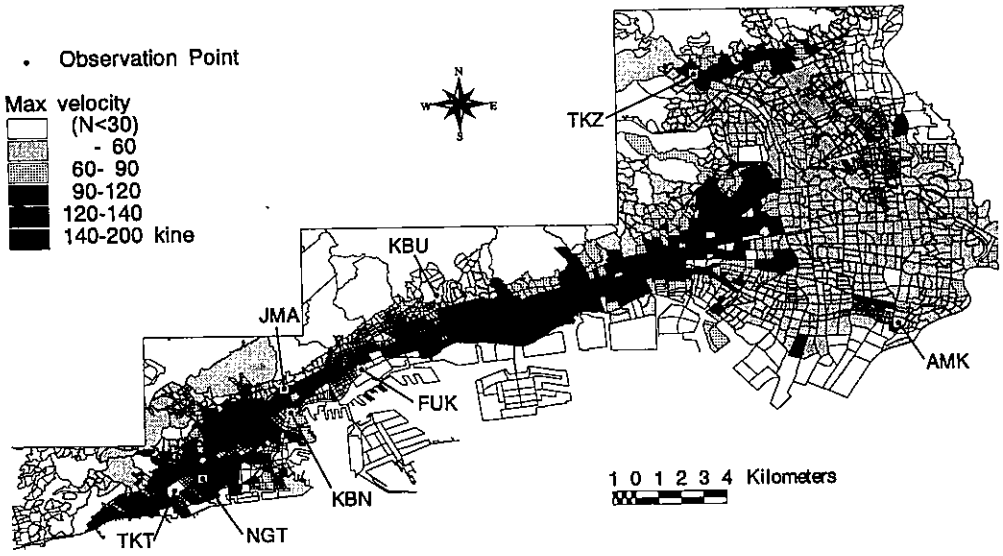

Fig. 18. Peak ground velocity evaluated from the damage ratio of low-rise buildings (Hayashi et al., 1997)

bandpass-filtered in the frequency range of 0.2–1.0 Hz. This distribution qualitatively resembles the peak velocity distribution evaluated from the damage ratio of the low rise buildings shown in Fig. 18 (Hayashi et al. [23]). The peak velocity distribution extending farther east seems to reflect the bedrock topography.

The dominance of fault-normal motions near the causative faults is a direct consequence of the directivity effects for the strike-slip fault as has been indicated by several authors. If the directivity effects only controlled the strong ground motions, the spatial pattern of the peak amplitudes would be symmetrical with respect to the fault traces; but, it is not. We consider that the concentration of the amplification within a limited area offset somewhat to the basin side originated from constructive interference between the seismic waves diffracted at the basin edges that proceeded into the basin and the direct incident S waves vertically propagating through the sediments from the basin bottom. This constructive interference, the so-called "basin edge effect" (Kawase[24]), is effective within a limited zone offset from the basin edge. The width of the zone and its distance from the edge depends on the frequency contents of the incident waves, the basin edge geometry, and the S wave velocities of the sediments.

The synthetic velocities are underestimated by factors of two to three, depending on stations. In this simulation we assumed a simplified basin structure consisting of a homogeneous sedimentary layer underlain by bedrock. The effects of the softer sedimentary layers on the ground motions in the Osaka basin are not negligible. We could examine the amplification produced by those soft layers beneath the stations as calculated from the one-dimensional velocity model. We conclude that the soft sedimentary layers, in addition to the basin edge effects in the Kobe area, contributed to ground motion amplification.

6. ESTIMATION OF GROUND MOTION AT HEAVILY DAMAGED SITES

One problem with this earthquake is that very few strong ground motions were recorded in the heavily damaged zones during the mainshock. Strong ground motion records are indispensable when discussing how buildings and bridges performed and why they reached to collapse. We

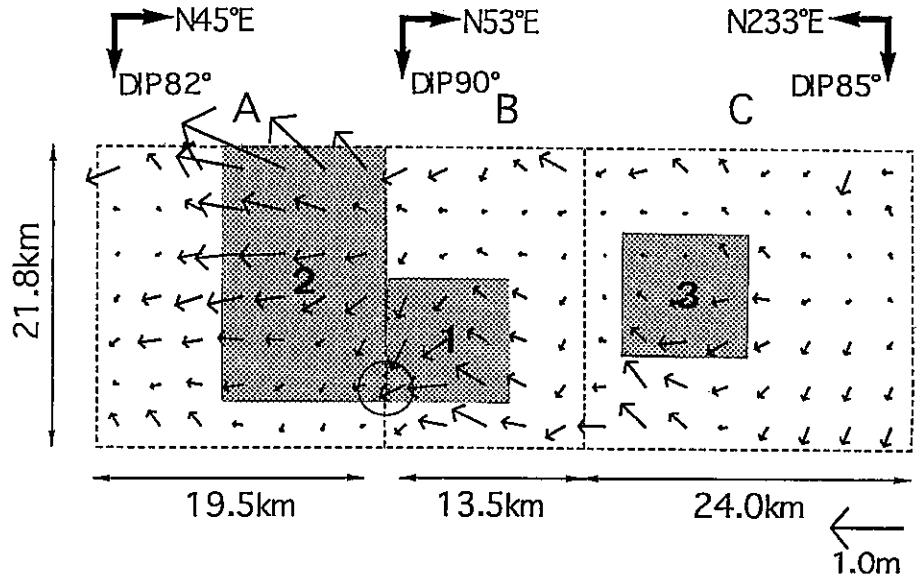

Fig. 19. Source model for simulating the mainshock using the empirical Green's function method. Three asperities (1, 2, and 3) are assumed on the basis of the distribution of the slip vectors from the waveform inversion shown by the arrows. Seismic waves are generated by only three events corresponding to the asperities. The parameters, strike, dip, moment, stress drop, and rise time are 233°, 90°, 0.34×10^{19} Nm, 16.3 MP, 0.6 sec, for event 1; 233°, 96°, 1.0×10^{19} Nm, 8.6 MP, 0.6 sec for event 2, and 233°, 85°, 0.18×10^{19} Nm, 8.6 MP, 0.6 sec,for event 3. Arrows showing total slip vector are obtained by Sekiguchi et al. [5].

therefore made aftershock observations at several sites in the heavily damaged areas of the basin as well as at rock sites at the foot of the Rokko mountain in Kobe as stated previously.

Irikura [25] developed a simulation method, the so-called empirical Green's function method (E.G.F. method) for strong ground motion that sums the records of small events on the fault plane of the mainshock to match the earthquake scaling laws of source parameters and source spectra. The E.G.F.method has been tested by many authors and shown to be a particularly good simulation technique if the source scaling and complexity of the rupture process are considered.

We made estimates of the ground motion at the severely damaged sites using aftershock records as the empirical Green's functions. There have been several determinations of the rupture model of this earthquake based on the inversion of the strong ground motion records (e.g. Sekiguchi, et al. [5]; Ide et al. [10], Yoshida et al. [11]; Wald [12]). The general features of those models are very similar each other. Models based on source inversion are not however always available for estimating strong ground motions that dominate high frequency motions because the inversion is made using displacement or velocity data that have been low-pass-filtered (about 1 Hz.).

We therefore tried to redetermine a source model that would be capable of estimating broader frequency motions that contain high frequency components of more than 1 Hz (Kamae and Irikura [26]). A source model for testing high frequency motions for engineering purposes must be as simple as possible in order to apply it to strong motion prediction for future earthquakes. Taking into account the inverted slip distribution, we assume a source model with three asperities. The contribution from the asperity in the deeper part of the Ashiya segment is

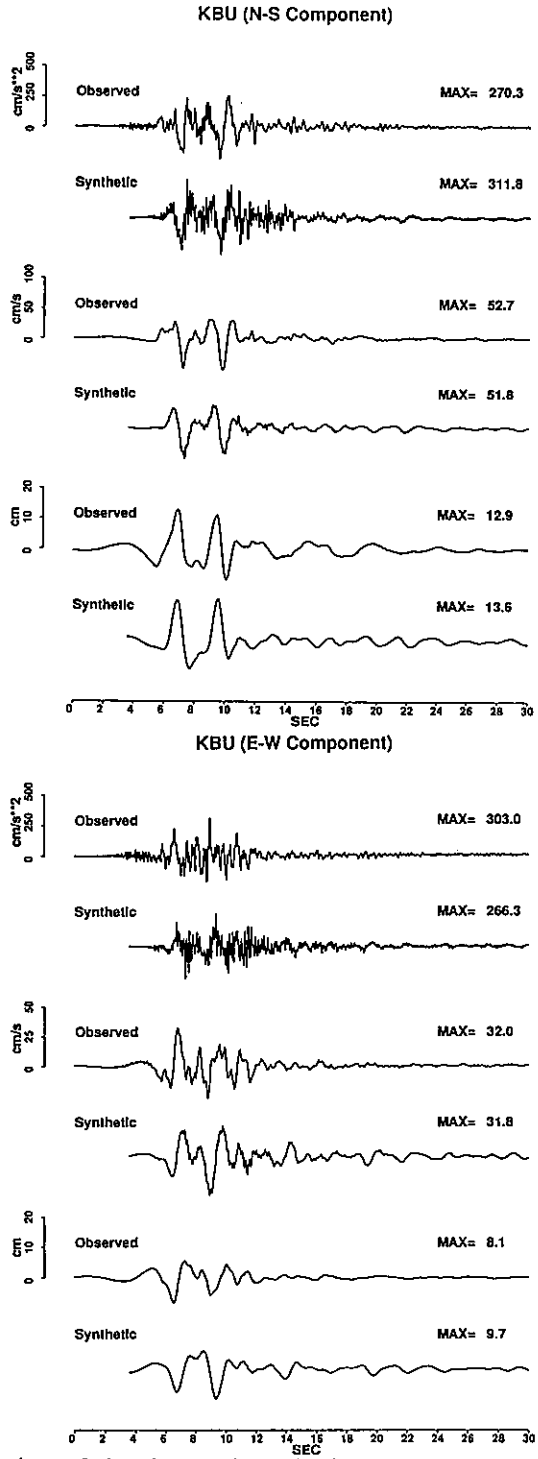

Fig. 20. Comparison of the observe observed seismograms (acceleration, velocity, and displacement) and synthesized ones using aftershock records. Left: Horizontal NS (upper) and EW (lower) components at KBU. Right: Horizontal NS (upper) and EW (lower) components at CHY.

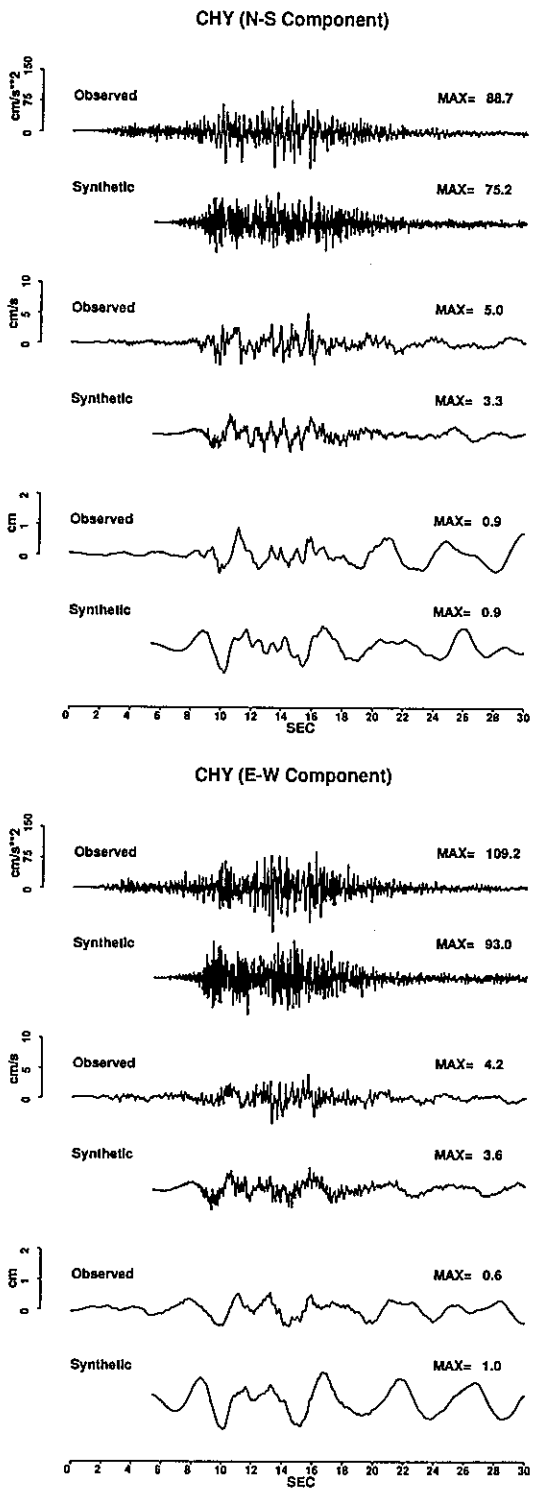

Fig. 20. (Continued.)

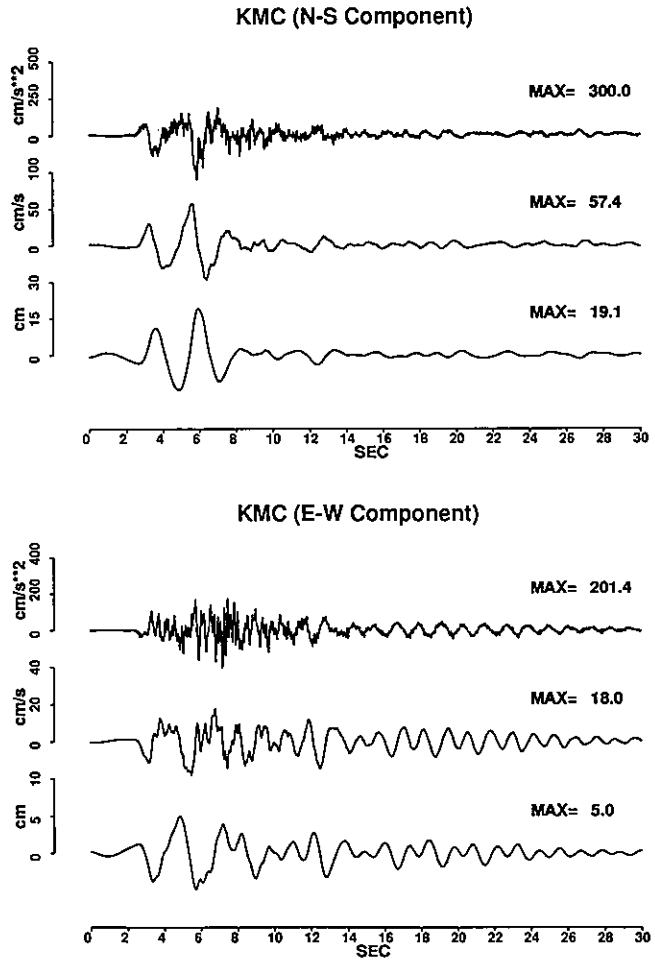

Fig. 21a. Simulated seismograms (acceleration, velocity, and displacement from upper) using aftershock records for the mainshock at KMC.

omitted because it has less effect on the strong pulses in Kobe area. Ground motions are generated only from the asperities with a certain constant stress drop. The stress drops of the three asperities are not identical.

First we estimated the ground motions for sites at which both the mainshock and aftershock records were recorded. After several trials and errors with forward modeling with respect to the depth and stress drop of each asperity, we obtained the best model that would fit the synthesized motions to the observed ones as shown by hatched area in Fig. 19. The source parameters for the respective asperities (hatched area) are given in the caption of Fig. 19. The synthesized motion for the mainshock is obtained by the summation of the respective motions generated from the three asperities.

The synthesized and observed motions at KBU, in a tunnel near rock very close to the causative faults, and at CHY, near an outcrop of rock 60 km east of the epicenter, are compared in Fig. 20. Both show a good agreement between the synthesized and observed values for velocity and displacement waveform, peak amplitude, and duration of acceleration. Although this source model seems to be a very simplified one, the synthesized and observed values at more than 8 stations ranging from a few kilometers to about 50 km from the epicenter are in good

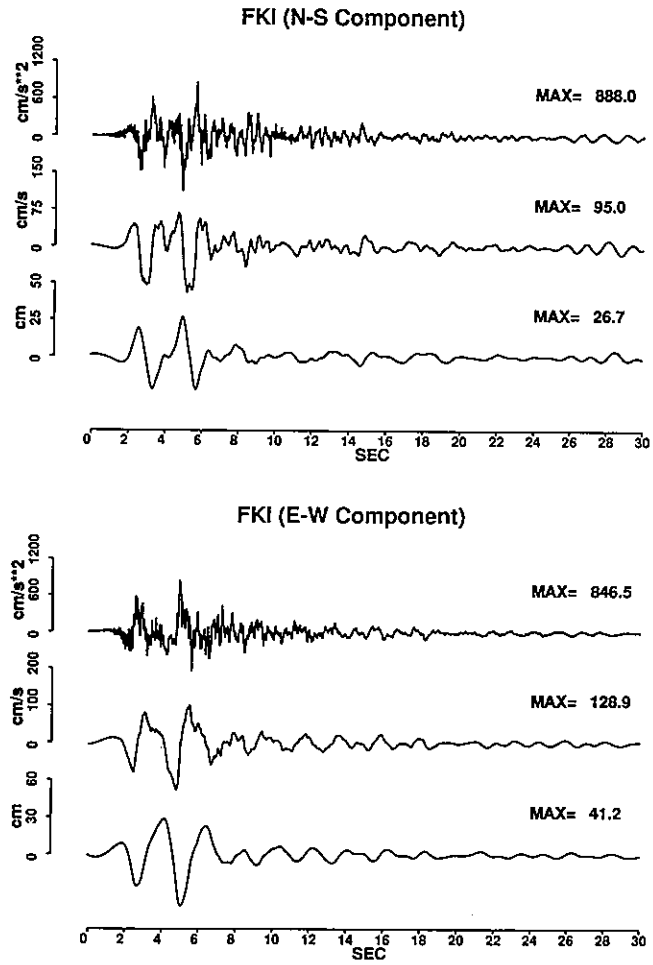

Fig. 21b. Simulated seismograms (acceleration, velocity, and displacement from upper) using aftershock records for the mainshock at FKI.

agreement. Synthetic accelerations at soft soil sites in the near-source distance show more high frequency motion than the observed accelerations, probably because of the non-linear behavior of the soft soil layers for strong ground motions (Aguirre and Irikura [21]).

Lastly, we estimated the strong ground motions at sites at which the mainshock was not recorded, using the aftershock records and the procedure described above. The aftershock records themselves at sites in the "Damage Belt" are affected by the basin edge effect as shown in Fig 14.

The synthesized ground motions are shown in Fig. 21a at KMC located near rock and in Fig. 21b, 21c at FKI and ASY in the heavily damaged area. For comparison, observed records at KOB, the JMA Kobe station situated on middle pleistocene deposits, are shown in Fig. 21d. The strong ground motions synthesized here as well as those observed at KBU and KOB in the near fault region were characterized by two, large, long-period pulses of 1 to 3 seconds. These large pulses predominate in the direction normal to the fault. Similar ground motion characteristics in the near-fault region had been observed in the 1994 Northridge, California, earthquake and the 1989 Loma Prieta earthquake (even though these earthquakes had different faulting mechanisms) that were indicative of forward rupture directivity on near-fault ground motion (Heaton et al. [2] and Somerville et al. [3]). Heaton et al.[3] warned that such ground motions caused major

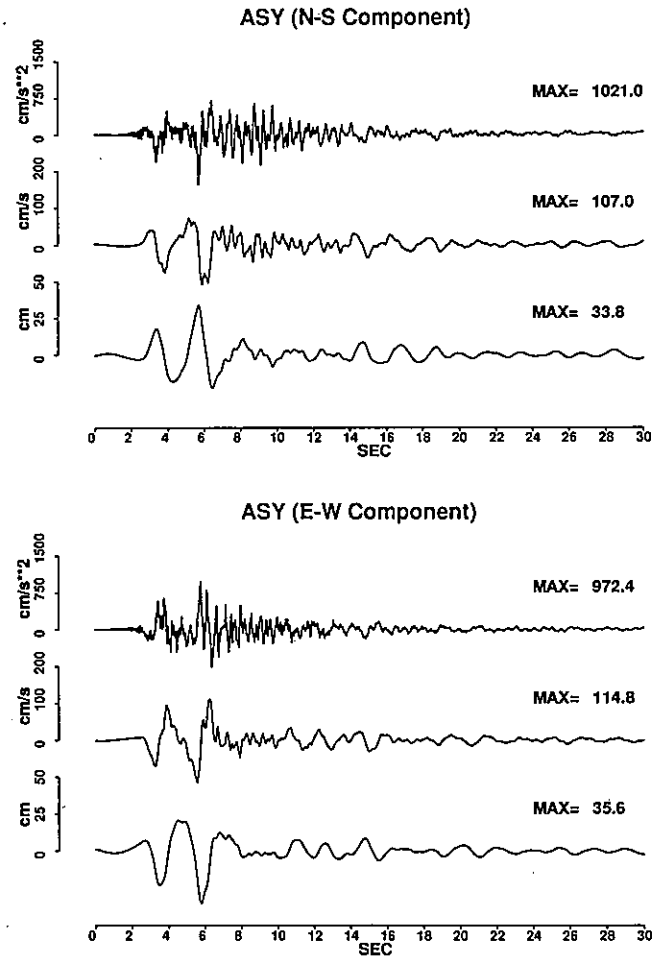

Fig. 21c. Simulated seismograms (acceleration, velocity, and displacement from upper) using aftershock records for the mainshock at ASY.

deformation and the possible collapse of frame buildings.

The respective peak horizontal acceleration and velocity of the synthesized motions at rock site KMC are about 300 gals and 57 cm/s, nearly the same as the values observed at rock site KBU. The respective peak accelerations of the synthesized motions at FKI and ASY in the heavily damaged area are about 900 and 1,000 gals, a little larger than the observed value (833 gals) at FKA (the Osaka Gas Corp, Fukiai office) located near the northern rim of the damaged area. The largest velocities of the synthesized motions at FKI and ASY,respectively, are about 130 and 115 cm/s, somewhat smaller than the observed value (138 cm/s, horizontal NS) at TKT (JR Takatori railway station) near the southern rim of the damaged area and a little larger than the observed value (121 cm/s, horizontal NS) at FKA. The response spectra at periods of 1 to 3 seconds at FKI and ASY are notably larger than those at KOB in the less damaged area. This difference between the damaged sites FKI and ASY and the less damaged site KOB is due to their relative locations from the basin's edge. That is, ground motions in the heavily damaged area have the large long-period pulses caused by the forward rupture directivity effects as well as the basin edge effects.

This appears to be the main cause of the damage being concentrated parallel to the fault but offset about 1 km southeast of it. The difference in response mentioned above may be related to

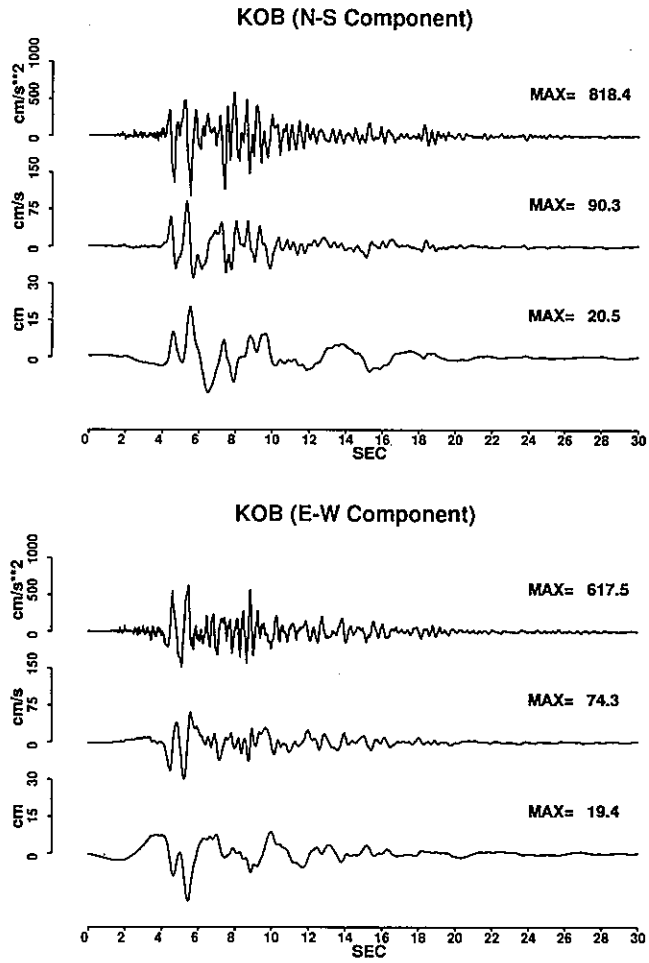

Fig. 21d. Observed seismograms (acceleration, velocity, and displacement from upper) from the mainshock at KOB.

the damaging effect of ground motions on buildings.

6. CONCLUSION

The surface traces of faulting in Kobe during the 1995 Hyogo-ken Nanbu earthquake were constrained by examining the particle motions of near-source strong motion records. The fault traces are consistent with the known active fault lines, but not with the heavily damaged zone. The rupture process from waveform inversion of the strong motion data shows concentrated slips in the shallow portion of the Nojima fault in Awaji Island, but only in the buried portions of the Rokko faults in the Kobe area. This coincides with surface breaks seen along the Nojima fault in Awaji Island, but not seen in Kobe.

The ground motions in the near-fault region in Kobe were characterized by two large-pulses with a duration of 1 to 2 seconds. These pulse durations are related to the sizes of the asperities obtained from the inverted slip distribution. In particular, ground motions near the heavily damaged zones have distinctive pulses that have higher amplifications larger than those in less damaged areas.

We simulated near-source ground motions using the 3-D finite difference method on the basis

of the slip distributions inverted from observed strong motion records and a 3-D velocity structure of the Kobe area determined with the seismic reflection method.
Impulsive ground motions of extremely high amplitude in the period range of 1 to 2 seconds were generated in narrow zones that coincide with the heavily damaged areas offset about 1 km from the Osaka basin's edges. This simulation explains the mechanism that produced the "Damage Belt". That is, strong pulses were generated from the forward rupture directivity in the near source area, which were further amplified due to the basin edge effects, thereby causing the disaster belt zone running that parallels the causative faults.

We estimated the strong ground motions at the heavily damaged sediment-sites and at undamaged rock sites in the near-source region, for which no mainshock records were recorded. The synthesized ground motions at the damaged and undamaged sites have two distinctive pulses, similar to the observed motion records, but the maximum amplitudes of those records markedly differ. The respective peak accelerations and velocities of the synthesized motions are about 1,000 gals and 130 cm/s at the heavily damaged sites and about 300 gals and 60 cm/s at the rock sites. We conclude that the destructive ground motions were caused by forward rupture directivity and the basin edge effects. Special notice therefore should be taken about ground motions amplified by the coupling of source and geological structure effects when mapping seismic hazards in urban areas.

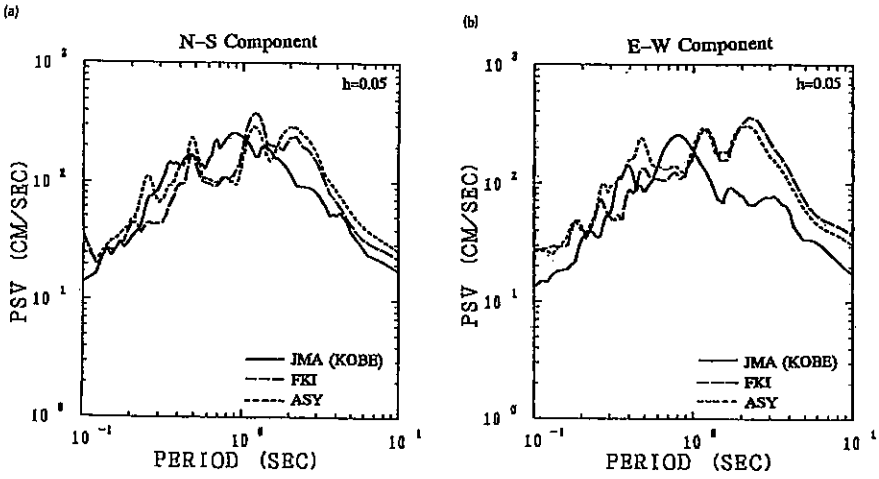

Fig. 22. Comparison of the pseudo velocity response spectra (PVRS) of the synthetic seismograms at FKI and ASY in seriously damaged areas ranked JMA Intensity 7 with the observed seismograms at KOB in a less damaged area ranked Intensity 6.

REFERENCES

[1] Nakata, T. and K. Yomogida (1995). Surface fault characteristics of the 1995 Hyogoken-nambu earthquake, J. Natural Disaster Science, 16-3, 1–10

[2] Heaton, T. H., J. F. Hall, D. J. Wald, M. W. Halling (1995). Response of high-rise and base-isolated buildings to hypothetical Mw 7.0 blind thrust earthquake, Science, 267, 206– 211.

[3] Somerville, P. G., N. F. Smith, R. W. Graves, and N. A. Abrahamson (1995). Accounting for near-fault rupture directivity effects in the development of design ground motion, Proceedings of the 1995 ASME/JSME PVP Conference, Hawaii, July 23–27.

[4] Sekiguchi, H., K. Irikura, T. Iwata, Y. Kakehi, M. Hoshiba (1996a). Determination of the location of faulting beneath Kobe during the 1995 Hyogo-ken Nanbu, Japan earthquake from near-source particle motion, Geophys. Res. Lett., 23, 387–390.

[5] Sekiguchi, H., K. Irikura, T. Iwata, Y. Kakehi, and M. Hoshiba (1996b). Minute locating of faulting beneath

Kobe and the waveform inversion of the source process during the Hyogo-ken Nanbu, Japan, earthquake using strong ground motion records, J. Physics of the Earth, 44, 473–488.

[6] Hashimoto, M., T. Sugita, H. Tsuji, Y. Hatanaka, and T. Tada (1996). Co-seismic Displacements of the 1995 Hyogo-ken Nanbu Earthquake, J. Physics of the Earth, 44, 255–280.

[7] Ozawa, S., M. Murakami, S. Fujiwara, T. Saito, M. Tobita, and M. Nemoto (1996). Geodetic inversion of the 1944 Hyogo-ken Nanbu earthquake -2, Programme and Abstracts of Seismological Society of Japan, No.2, A40.

[8] Koketsu K., S. Yoshida, T. Uetake, and T. Furumura (1996). A fault model of the 1995 Kobe earthquake derived from geodetic, teleseismic, and damage distribution data, Programme and Abstracts of Seismological Society of Japan, No.2, A41.

[9] Hartzell, S. H. and T. H. Heaton (1983). Inversion of strong ground motion and teleseismic waveform data for the fault rupture history of the 1979 Imperial Valley, California earth-quake, Bull. Seism. Soc. Am., 73, 1553–1583.

[10] Ide, S., M. Takeo, and Y. Yoshida (1996). Source Model of the 1995 Hyogo-ken Nanbu earthquake determined by near-field strong-motion records, J. Phys. Earth, 44, 649–655.

[11] Yoshida S., K. Koketsu, B. Shibazaki, T. Sagiya, T, Kato, and Y. Yoshida (1996). Joint inversion of near-and far-field waveforms and geodetic data for the rupture process of the 1995 Kobe earthquake, J. Physics of the Earth, 44, 437–455.

[12] Wald, J. D. (1996). Slip history of the 1995 Kobe, Japan, Earthquake determined from strong ground motions, teleseismic, and geodetic data, J. Physics of the Earth, 44, 489–504.

[13] Iwata, T., K. Hatayama, H. Kawase, K.Irikura, and K. Matsunami (1995). Array observation of aftershocks of the 1995 Hyogo-ken Nanbu earth-quake at Higashinada Ward, Kobe city, Journal of Natural Disaster Science, 16–2, 41–48.

[14] Kagawa, T., S. Sawada, Y. Iwasaki, and A. Nanso (1993). Modeling of deep sedimentsry structure beneath the Osaka basin, Proc. 22th JSCE Earthquake Engineering Symposium, 199–202 (in Japanese).

[15] Pitarka, A. and K. Irikura (1996). Basin structure effects on long period strong motions in the San Fernando valley and in the Los Angeles basin from the 1994 Northridge earthquake and an aftershock, Bull. Seis. Soc. Am., 86, S126–S137.

[16] Pitarka, A., K. Irikura, T. Iwata, and T. Kagawa (1996). Basin structure effects in the Kobe are inferred from the modeling of ground motions from two aftershocks of the January 17, 1995, Hyogo-ken Nanbu earthquake, J. Physics of the Earth, 44, 563– 576.

[17] Geological Survey of Japan (1996). Reports on surveys of active fault in 1995, 85 (1n Japanese).

[18] Iwata, T., K. Hatayama, H. Kawase, and K. Irikura (1996). Site amplification of ground motions during aftershocks of the 1995 Hyogo-ken Nanbu earthquake in severely damaged zone, J. Phys. Earth, 44, 553–562.

[19] Kobayashi, S., S. Yoshida, S. Okubo, R. Shichi, T. Shimamoto, and T. Kato (1996). 2.5-Dimensional analysis of gravity anomaly across the Rokko fault system, J. Phys. Earth, 44, 357–372.

[20] Nakagawa, K., K. Shiono, N. Inoue, and M. Sano (1996). Geological characteristics and problems in and around Osaka basin as a basis for assessment of seismic hazards, Soils and Foundations, Japan, 15–28.

[21] Aguirre, J. and K. Irikura(1995). Preliminary analysis of non-linear site effects at Port Island Vertical Array Station during the 1995 Hyogo-ken Nanbu earthquake at Higashinada Ward, Kobe city, Journal of Natural Disaster Science, 16–2, 49–58.

[22] Pitarka, A. and K. Irikura (1996). Modeling 3D surface topography by finite-difference method: Kobe-JMA station site, Japan, case study, Geophy. Res. Lett., 23, 2729–2732.

[23] Hayashi Y. J. Miyakoshi, K. Tamura, and K. Kawase (1997). Peak ground velocity evaluated from damage ratios of low-rise buildings during the Hyogo-ken Nanbu earthquake of 1995, J. Struct. Constr. Eng., AIJ, No.494, 59–66.

[24] Kawase, H. (1996). The cause of the damage belt in Kobe: "The basin-edge effect", constructive interference of the direct S-wave with the basin-induced diffracted/Rayleigh waves, Seism. Res. Let., 67–5.

[25] Irikura, K. (1986). Prediction of strong acceleration motion using the empirical Green's function, Proc.7th Japan Earthq. Eng. Symp., 151–156.

[26] Kamae, K. and Kojiro Irikura (1997). A fault model of the 1995 Hyogo-ken Nanbu earthquake and simulation of strong ground motion in near-source area, J. Struct. Constr. Eng. (Trans. AIJ), in press.